Strain rate effects on the mechanical behavior of thick-walled pressurized cylinders

Andrey Brezolin[1], Tiago dos Santos[2], Rodrigo Rossi[1]

[1]*Dept. of Mechanical Engineering, Federal University of Rio Grande do Sul*
Sarmento Leite, 425, Porto Alegre, 90.050-170, RS, Brazil
andreybrezolin@gmail.com, rrossi@ufrgs.br
[2]*Dept. of Mechanical Engineering, Federal University of Santa Maria*
Av. Roraima, 1000, Santa Maria, 97105-900, RS, Brazil
tiago.santos@ufsm.br

Abstract. This work studies strain rate effects on the mechanical behavior of thick-walled cylinders subjected to internal pressure. The material is assumed to present an elastic-viscoplastic behavior presenting strain hardening, strain rate hardening and instantaneous rate sensitivity. In an effort to elucidate the expected strain rate effects, the thick-walled cylinder is assumed to radially expand due to an imposed displacement on its internal surface. The influence of the imposed expansion velocity on the mechanical field that develops through the thickness is assessed by means of an analytical solution and using finite element simulations. The analysis considers constant velocity expansions and tests in which the expansion velocity is abruptly changed: stopped, decreased or increased. Such imposed loading conditions allow evidencing instantaneous and strain rate history effects on the stress response and on the material hardening behavior.

Keywords: Thick-walled cylinder, Strain rate effects, Elastic-viscoplastic material, Finite element analysis

1 Introduction

The mechanical analysis of pressurized thick-walled cylinders and spheres has been of great importance to many engineering applications, such as in the design of pressure vessels, pipelines, weapons, among others. In many of these applications, the structures can be exposed to dynamic loads, e.g., under blast or explosive conditions (Gerasimov, 2003; Elek et al., 2013). In this scenario, understanding the mechanical performance of thick-walled construction under dynamic conditions is of great relevance. Many efforts have been made to study the time-dependent response of viscoplastic hollow cylinders and spheres under dynamic deformation. Peirce et al. (1984) performed numerical analysis on elastic-viscoplastic pressurized cylinders, considering two limiting circumstances, the rate-independent limit and the power law creep limit. Haghi and Anand (1991) developed closed-form solutions to externally pressurized thick-walled spheres and cylinders, made of strain-hardening viscoplastic material. Li and Fu (2008) estimated plastic limit loads to internally pressurized viscoplastic thick-walled cylinders and spheres. They employed a strain gradient plasticity theory in order to capture the size effects. Their results demonstrated that the size effects increase with strain or strain rate-sensitivity. Gerasimov (2003) developed a theoretical model to expanding elastic-plastic thick-walled cylinders under shock loading. Damage conditions were also accounted for in their modeling framework. Bagheri et al. (2017) presented a dynamic analysis regarding the mechanical behavior of a thick-walled cylinders considering nonlinear strain rate hardening. Using a theoretical model, a detailed analysis on the developed mechanical field, considering different strain rate sensitivities, was provided by the authors. Kats and Morozov (2020) studied the deformation and fracture of thick-walled composite cylinders subjected explosive conditions. Estimates of the failure stresses of the composite material were provided. In this work, we study strain rate effects on the mechanical behavior internally pressurized thick-walled cylinders. An elastic-viscoplastic material, presenting strain hardening, strain rate hardening and instantaneous rate-sensitivity, is assumed. By means of both theoretical and numerical analysis instantaneous strain rate-sensitivity and strain rate history effects are investigated.

2 Constitutive model

This section briefly outlines the main feature of the elastic-viscoplastic model (dos Santos et al., 2016) adopted in this work. It is assumed that the material follows the von Mises yield condition:

$$f(\boldsymbol{\sigma}, A) = \|\mathbf{s}\| - \sqrt{2/3}\,(\sigma_y + A)\,, \tag{1}$$

where σ_y is the initial yield stress, $||\mathbf{s}|| = \sqrt{\mathbf{s} : \mathbf{s}} = \sqrt{s_{ij}s_{ij}}$, being $\mathbf{s}$ the deviatoric part of the Cauchy stress tensor $\boldsymbol{\sigma}$. Furthermore, A is an isotropic stress-like variable, which is assumed to result from two distinct contributions: $A = A_1 + A_2$. The first one accounts for the nonlinear hardening at earlier deformation and the second one for the subsequent linear branch. Assuming an elastic-viscoplastic material under small strains, the total strain tensor $\boldsymbol{\varepsilon}$ is decomposed into its elastic and viscoplastic parts:

$$\boldsymbol{\varepsilon} = \boldsymbol{\varepsilon}^e + \boldsymbol{\varepsilon}^{vp}. \tag{2}$$

It is assumed that the stress tensor $\boldsymbol{\sigma}$ and the elastic strain tensor $\boldsymbol{\varepsilon}^e$ are related as:

$$\boldsymbol{\sigma} = \mathbf{D}^e\boldsymbol{\varepsilon}^e, \tag{3}$$

being $\mathbf{D}^e = 2\mu\mathbf{I} + \lambda\mathbf{I}\otimes\mathbf{I}$ the fourth-order isotropic elastic tensor, where μ and λ are Lamé constants, $\mathbf{I}$ and $\mathbf{I}$ are the fourth and second-order identity tensors, respectively, such that: $\mathbf{I}_{ijkl} = \frac{1}{2}\left(\delta_{ik}\delta_{jl} + \delta_{il}\delta_{jk}\right)$ and $(\mathbf{I}\otimes\mathbf{I})_{ijkl} = \delta_{ij}\delta_{kl}$. The viscoplastic strain rate and the hardening variables evolution are assumed to respect the following relations:

$$\dot{\boldsymbol{\varepsilon}}^{vp} = \dot{\lambda}\frac{\partial f}{\partial \boldsymbol{\sigma}}, \qquad \dot{A}_1 = \delta\left(A_\infty - A_1\right)\dot{\bar{\varepsilon}}, \qquad A_2 = cA_\infty\bar{\varepsilon}, \tag{4}$$

where $\dot{\lambda}$ is a non-null viscoplastic multiplier, δ, A_∞ and c are model parameters, $\bar{\varepsilon}$ is the accumulated viscoplastic strain, whose rate is relates with $\dot{\lambda}$ by: $\dot{\bar{\varepsilon}} = \sqrt{2/3}\dot{\lambda}$. In an effort to account for strain rate history effects, parameter A_∞ in Eq. (4) is assumed to be rate-dependent:

$$A_\infty = A_\infty^{lwr} + \left(\frac{\left\langle\dot{\bar{\varepsilon}} - \dot{\bar{\varepsilon}}_{lwr}\right\rangle}{\dot{\bar{\varepsilon}}_{up} - \dot{\bar{\varepsilon}}_{lwr}}\right)^{\xi}\left(A_\infty^{up} - A_\infty^{lwr}\right), \tag{5}$$

where $\langle x\rangle = \frac{1}{2}\left(x + |x|\right)$, $\xi > 0$ is a model constant, A_∞^{lwr} and A_∞^{up} are the values of A_∞ at reference strain rates, $\dot{\bar{\varepsilon}}_{lwr} \ll 1$ and $\dot{\bar{\varepsilon}}_{up} \gg 1$, respectively. The instantaneous strain rate-sensitivity is modeled using an overstress framework (Perzyna, 1971). Therefore, during plastic loading, the yield function (f) relates to the viscoplastic multiplier $\left(\dot{\lambda}\right)$ by means of: $f = \Theta^{-1}\left(\dot{\lambda}, A\right)$. Here, the overstress function Θ^{-1} proposed by Perić (1993) is adopted:

$$f = \sqrt{2/3}\,(\sigma_y + A)\left[\left(1 + \vartheta\dot{\lambda}\right)^{1/m} - 1\right], \tag{6}$$

where and $1/m > 0$ are constants.

3 Thick-walled cylinder analysis

This section outlines the mechanical problem to be addressed in this work. It consists of thick-walled cylinder subjected to uniform radial displacement $\bar{u}_r$ on its internal radius, $r = a$. The imposed displacement tends to mimic the effect of the internal pressure using a kinematic approach, while the outer radius $(r = b)$ is pressure-free. The problem is illustrated in Fig. 1. The cylinder's material is assumed to follow the constitutive behavior described in previous section.

Given the cylindrical symmetry of this problem (see Fig. 1), assuming that the cylinder expands at a constant velocity $\bar{v}$ and that the material is rigid-viscoplastic, a plane strain solution can be obtained, providing the distribution of the radial (σ_{rr}), circumferential $(\sigma_{\theta\theta})$ and longitudinal (σ_{zz}) stresses, respectively (see Brezolin (2018)):

$$\sigma_{rr} = \frac{2}{\sqrt{3}}\left[\sigma_y\int_b^r\left(\xi^2 + \vartheta\sqrt{2}\bar{v}a\right)^{1/m}\xi^{-(2+m)/m}d\xi + \int_b^r A\left(\xi^2 + \vartheta\sqrt{2}\bar{v}a\right)^{1/m}\xi^{-(2+m)/m}d\xi\right], \tag{7}$$

$$\sigma_{\theta\theta} = \frac{2}{\sqrt{3}}\left(\sigma_y + A\right) + \sqrt{2}\Theta^{-1} + \sigma_{rr}, \tag{8}$$

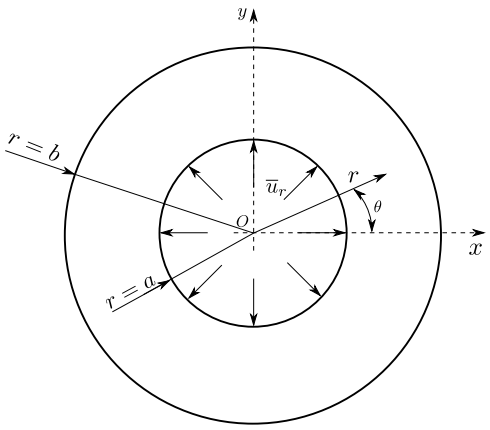

Figure 1: Schematic representation of the thick-walled problem in a two dimensional space.

$$\sigma_{zz} = \frac{\sigma_{rr} + \sigma_{\theta\theta}}{2}. \tag{9}$$

The related internal pressure can be canculated as:

$$p_i = -\sigma_{rr}\left(a\right). \tag{10}$$

Moreover, given the stress components in Eqs. (7)-(9), the von Mises equivalent stress is then calculated:

$$\sigma_{vM} = \sqrt{\frac{1}{2}\left[\left(\sigma_{rr} - \sigma_{\theta\theta}\right)^2 + \left(\sigma_{\theta\theta} - \sigma_{zz}\right)^2 + \left(\sigma_{zz} - \sigma_{rr}\right)^2\right]}. \tag{11}$$

3.1 Finite element model

The axisymmetric finite element model used to simulate the thick-walled cylinder expansion in shown in Fig. 2, where the dimensions are also provided. A radial displacement of $\bar{u}_1 = 1\,\mathrm{mm}$ is imposed on the inner radius at different velocities $\bar{v}$, thus providing different strain rates through the thickness. The finite element model was built in ABAQUS/Standard, using 20 eight-node elements (CAX8R) with reduced integration. The constitutive model outlined in section 2 was implemented in a user subroutine (UMAT). See dos Santos et al. (2017) and Brezolin et al. (2019) for details on the numerical formulation. Model parameters used in the simulations are in Table 1.

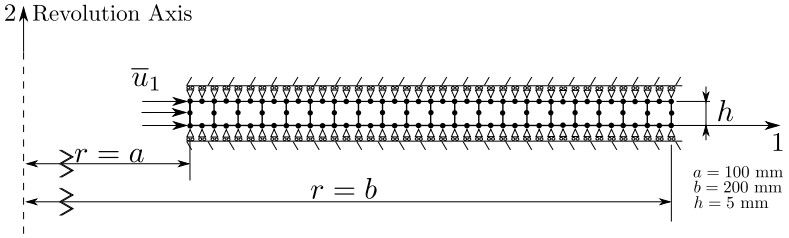

Figure 2: Thick Walled Cylinder - Geometry, boundary conditions and finite element mesh.

Table 1: Model parameters used in the simulations, with $\dot{\bar{\varepsilon}}_{lwr} = 10^{-4}$ and $\dot{\bar{\varepsilon}}_{up} = 10^{4}\ \mathrm{s}^{-1}$ (after dos Santos et al. (2016)).

E	ν	σ_y	δ	c	A_∞^{lwr}	A_∞^{up}	ξ	ϑ	m
(GPa)	-	(MPa)	-	-	(MPa)	(MPa)	-	(s)	-
112	0.33	35	6.46	0.42	233	420	3.16	1.2×10^3	105

4 Results

This sections presents the finite element results for two distinct conditions: (i) the cylinder expands at a constant velocity $\bar{v}$ and then the expansion is abruptly stopped; and (ii) sequential tests, in which, the expansion velocity is abruptly increased or decreased at a given time. The first scenario is considered in order to evidence the instantaneous rate-dependence, while the second test evidences strain rate history effects on the mechanical behavior.

4.1 Instantaneous rate-sensitivity

In this case, the cylinder expands at a constant velocity $\bar{v}$ until reaching a radial displacement of $\bar{u}_r = 1\,\mathrm{mm}$ at a time t_f. After that, the velocity is abruptly decreased to zero resulting in a stress relaxation process. Four distinct velocities are considered: 8.7×10^{-2}, 8.7×10^{1}, 8.7×10^{4}, and $8.7 \times 10^{5}\,\mathrm{mm/s}$. As it is shown in Fig. 3, these velocities provide the following accumulated viscoplastic strain rates at the inner radius: 10^{-2}, 10^{0}, 10^{2}, and $10^{4}\,\mathrm{s}^{-1}$, respectively. It is clearly seen that the strain rates slightly decrease with the dimensionless radial position r/a, to the respective values: 2.5×10^{-3}, 2.5×10^{-1}, 2.5×10^{1}, and $2.5 \times 10^{3}\,\mathrm{s}^{-1}$.

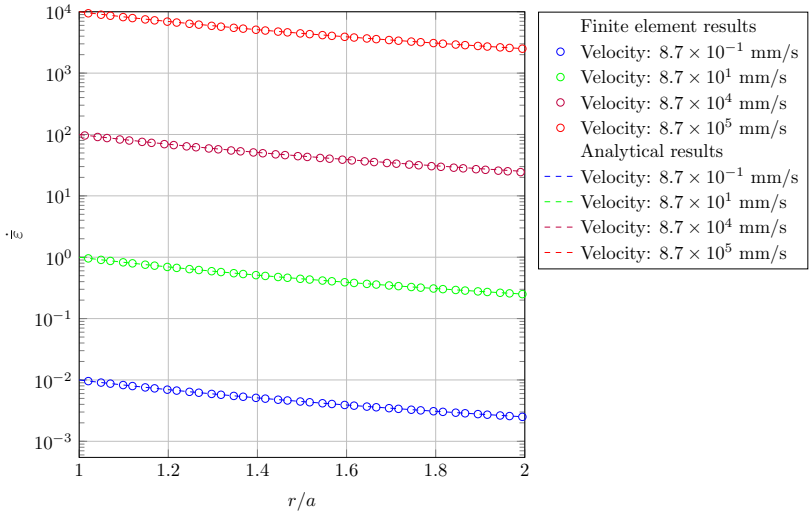

Figure 3: Accumulated viscoplastic strain rate $\dot{\bar{\varepsilon}}$ vs. the dimensionless radial coordinate r/a considering four expansion velocities, 8.7×10^{-2}, 8.7×10^{1}, 8.7×10^{4}, and $8.7 \times 10^{5}\,\mathrm{mm/s}$, at $t = t_f$.

Figure 4 shows the distribution of the dimensionless radial stress σ_{rr}/σ_y along the dimensionless radial coordinate r/a considering the four expansion velocities. While Fig. 4(a) shows the stress distribution in the end of the loading phase $(t = t_f)$, Fig. 4(b) gives the asymptotic response of the stress relaxation process. In both cases, the stress distribution has a concave downward shape and the absolute value of the radial stress increase with the imposed velocity. At $t = t_f$ (Fig. 4(a)), $|\sigma_{rr}(a)|/\sigma_y$ ranges from ≈ 1.00, for the smallest velocity, to ≈ 1.20, for the greatest loading rate. Comparing Figs. 4(a) and 4(b), the stress relaxation is readily observed, such that $|\sigma_{rr}(a)|/\sigma_y$ decreases from ≈ 1.20 to ≈ 1.15, for $\bar{v} = 8.7 \times 10^{5}\,\mathrm{mm/s}$. Less pronounced stress relaxation effects are observed for lower imposed velocities. Figure 4(a) also shows a good agreement between finite element and theoretical (Eq. (7)) results for all imposed velocities.

Figure 5 shows the distribution of the dimensionless von Mises equivalent stress σ_{vM}/σ_y along the dimensionless radial coordinate r/a considering the four expansion velocities, at different time instants: $t = t_f$ (Fig. 5(a)) and after stress relaxation (Fig. 5(b)). Similar tendencies to those of Fig. 4 are observed. The stress distribution has a concave upward shape and the equivalent stress increase with the imposed velocity. At $t = t_f$ (Fig. 5(a)), $\sigma_{vM}(a)/\sigma_y$ ranges from ≈ 1.52, for $\bar{v} = 8.7 \times 10^{-2}\,\mathrm{mm/s}$, to ≈ 2.10, for $\bar{v} = 8.7 \times 10^{5}\,\mathrm{mm/s}$. Stress relaxation is noticed while com comparing Figs. 4(a) and 4(b). During stress relaxation, the dimensionless equivalent stress at the inner radius reduces from ≈ 2.15 to ≈ 2.00, for the highest velocity. Again, less pronounced stress relaxation is observed as the loading rate decreases. In Figure 5(a), a good agreement is also observed while comparing finite element and theoretical (Eq. (11)) results.

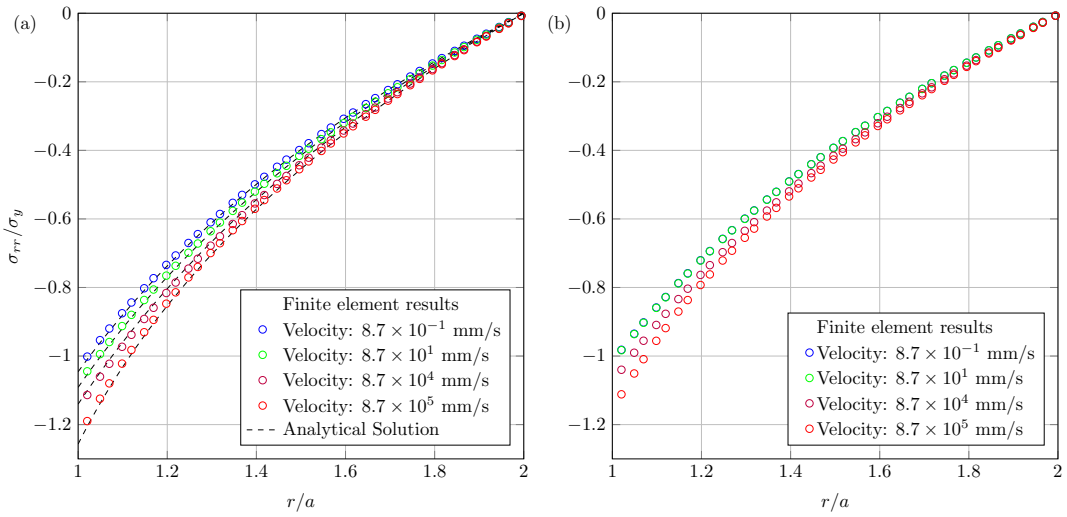

Figure 4: Dimensionless radial stress σ_{rr}/σ_y vs. the dimensionless radial coordinate r/a considering four expansion velocities, 8.7×10^{-2}, 8.7×10^{1}, 8.7×10^{4}, and $8.7 \times 10^{5}\,\mathrm{mm/s}$, at different time instants: (a) $t = t_f$ and (b) after stress relaxation. The analytical results (dashed lines) are obtained using Eq. (7).

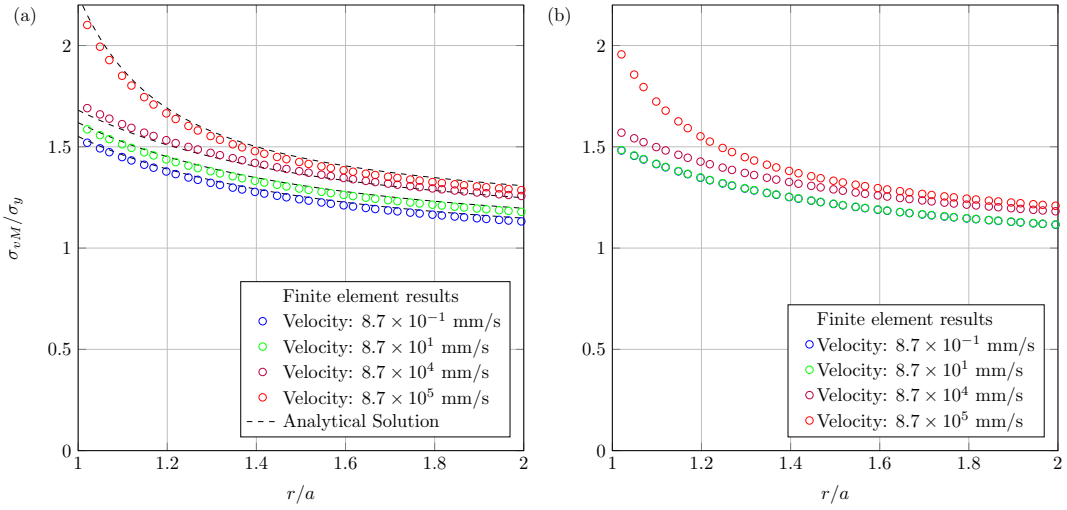

Figure 5: Dimensionless von Mises equivalent stress σ_{vM}/σ_y vs. the dimensionless radial coordinate r/a considering four expansion velocities, 8.7×10^{-2}, 8.7×10^{1}, 8.7×10^{4}, and $8.7 \times 10^{5}\,\mathrm{mm/s}$, at different time instants: (a) $t = t_f$ and (b) after stress relaxation. The analytical results (dashed lines) are obtained using Eq. (11).

4.2 Strain rate history effects

This section presents sequential simulations, in which the expansion velocity is abruptly decreased or increased. These tests are considered in order to evidence strain rate history effects on the mechanical behavior. Such an effects results from the strain rate-dependence of the material hardening evolution, see Eqs. $(4)_2$ and (5). Figure 6(a) shows the absolute value of the dimensionless radial stress $|\sigma_{rr}(a)|/\sigma_y$ in terms of the accumulated viscoplastic strain $\bar{\varepsilon}$ at the inner radius. When $\bar{\varepsilon} \approx 5.3 \times 10^{-3}$, the expansion velocity $\bar{v}$ is abruptly reduced from 8.7×10^{5} to $8.7 \times 10^{-2}\,\mathrm{mm/s}$, resulting in a sudden decrease in the strain rate at the inner radius, from 10^{4} to $10^{-2}\,\mathrm{s}^{-1}$. Due to this strong reduction in the loading rate, the dimensionless radial stress $|\sigma_{rr}(a)|/\sigma_y$ suddenly decreases from ≈ 1.05 to ≈ 0.92, due to instantaneous strain rate effects. However, it is noticed that the reduced stress is approximately 2.67% higher than the corresponding value in the curve obtained at a constant strain rate of $10^{-2}\,\mathrm{s}^{-1}$. This difference is the result of the strain rate history on the material hardening evolution. This behavior is also evidenced in Fig. 6(a), where the expansion velocity $\bar{v}$ jumps from 8.7×10^{5} to $8.7 \times 10^{-2}\,\mathrm{mm/s}$, suddenly increasing the strain rate at the inner radius, from 10^{-2} to $10^{4}\,\mathrm{s}^{-1}$. In this case, the dimensionless radial stress $|\sigma_{rr}(a)|/\sigma_y$ instantaneously goes from ≈ 0.90 to ≈ 1.03. However, the jump curve does not reach that obtained at a constant strain rate of $10^{4}\,\mathrm{s}^{-1}$.

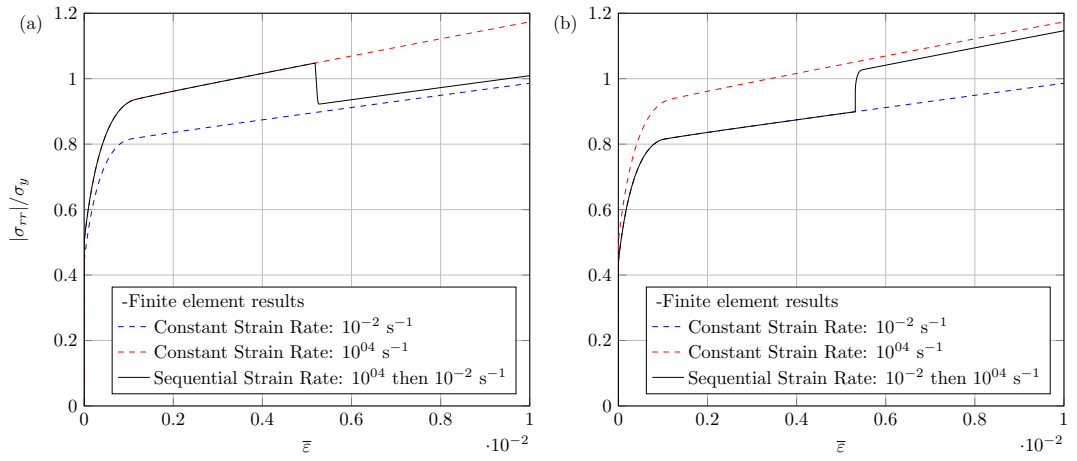

Figure 6: Dimensionless radial stress $|\sigma_{rr}(a)|/\sigma_y$ vs. the accumulated viscoplastic strain $\bar{\varepsilon}$ at the inner radius, considering (a) an abrupt reduction, from 10^4 to $10^{-2}\,\mathrm{s}^{-1}$, and (b) a jump, from 10^{-2} to $10^4\,\mathrm{s}^{-1}$, in the strain rate $\dot{\bar{\varepsilon}}$. Constant strain rate curves, for $\dot{\bar{\varepsilon}} = 10^{-2}\,\mathrm{s}^{-1}$ and $\dot{\bar{\varepsilon}} = 10^4\,\mathrm{s}^{-1}$, are also plotted for comparison purposes.

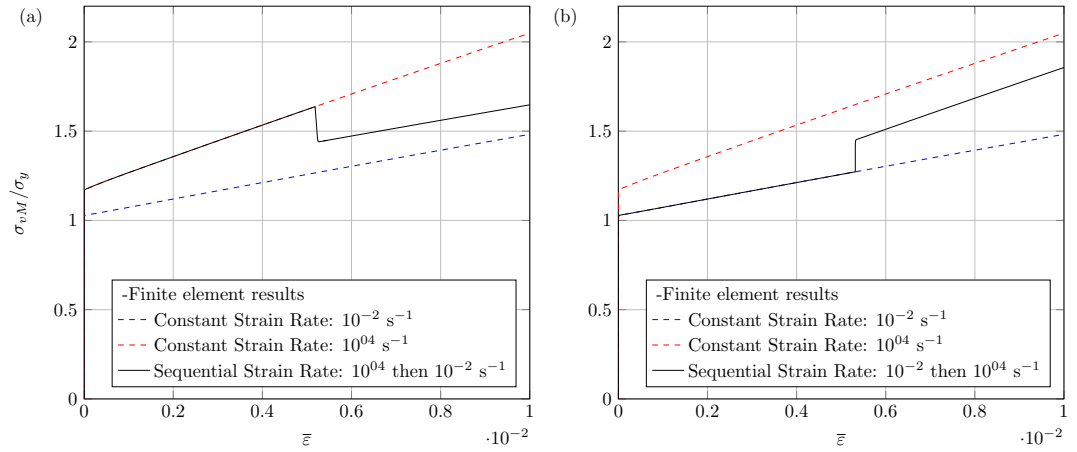

Figure 7: Dimensionless von Mises equivalent stress $\sigma_{vM}(a)/\sigma_y$ vs. the accumulated viscoplastic strain $\bar{\varepsilon}$ at the inner radius, considering (a) an abrupt reduction, from 10^4 to $10^{-2}\,\mathrm{s}^{-1}$, and (b) a jump, from 10^{-2} to $10^4\,\mathrm{s}^{-1}$, in the strain rate $\dot{\bar{\varepsilon}}$. Constant strain rate curves, for $\dot{\bar{\varepsilon}} = 10^{-2}\,\mathrm{s}^{-1}$ and $\dot{\bar{\varepsilon}} = 10^4\,\mathrm{s}^{-1}$, are also plotted for comparison purposes.

The same loading conditions of Fig. 6 were imposed to obtain the sequential strain rate curves shown in Fig. 7, which shows the dimensionless equivalent von Mises stress $\sigma_{vM}(a)/\sigma_y$ vs. the accumulated viscoplastic strain $\bar{\varepsilon}$ at the inner radius. While Fig. 7(a) shows the curve of an decremental strain rate test (from 10^4 to $10^{-2}\,\mathrm{s}^{-1}$), Fig. 7(b) displays the strain rate jump case (10^{-2} to $10^4\,\mathrm{s}^{-1}$). As in Fig. 6, the stress response abruptly decreases (Fig. 7(a)) or increases (Fig. 7(a)) with the sudden changes in the strain rate, which is the result of instantaneous rate effects. In contrast, the sequential tests do not reach the corresponding constant strain rate curves, evidencing the effects of the past loading rate on the material hardening.

5 Conclusions

This work has studied strain rate effects on the mechanical behavior of internally pressurized thick-walled cylinders. An elastic-viscoplastic material, presenting strain hardening, strain rate hardening and instantaneous rate-sensitivity, was adopted. Considering different loading rates, the influence of the imposed expansion velocity on the mechanical behavior was shown, using both analytical and finite element simulations. Obtained results evidenced both instantaneous and past strain rate effects on the stress response, showing the influence of the imposed loading conditions on the material/structure behavior.

Acknowledgements. AB wishes to acknowledge the fellowship from CAPES, Coordenação de Aperfeiçoamento

de Pessoal de Nível Superior. TdS wishes to acknowledge the support of FAPERGS, Fundação de Amparo à Pesquisa do Estado do Rio Grande do Sul, grant agreement 21/2551-0000744-3. RR wishes to acknowledge the support of *CNPq*, Conselho Nacional de Desenvolvimento Científico e Tecnológico, grant number 306058/2018-9.

Authorship statement. The authors hereby confirm that they are the sole liable persons responsible for the authorship of this work, and that all material that has been herein included as part of the present paper is either the property (and authorship) of the authors, or has the permission of the owners to be included here.

References

A. Gerasimov. Explosive deformation and fracture of thick-wall cylinders. *Strength of materials*, vol. 35, n. 2, pp. 162–167, 2003.

P. Elek, S. Jaramaz, and D. Mickovic. Modeling of the metal cylinder acceleration under explosive loading. *Sci. Tech. Rev*, vol. 63, n. 2, pp. 39–46, 2013.

D. Peirce, C. Shih, and A. Needleman. A tangent modulus method for rate dependent solids. *Computers & Structures*, vol. 18, n. 5, pp. 875–887, 1984.

M. Haghi and L. Anand. Analysis of strain-hardening viscoplastic thick-walled sphere and cylinder under external pressure. *International journal of plasticity*, vol. 7, n. 3, pp. 123–140, 1991.

M.-l. Li and M.-f. Fu. Limit analysis of viscoplastic thick-walled cylinder and spherical shell under internal pressure using a strain gradient plasticity theory. *Applied Mathematics and Mechanics*, vol. 29, n. 12, pp. 1553–1559, 2008.

S. M. Bagheri, J. Zamani, and M. H. Ghezelayagh. Dynamic expansion modeling of a thick-walled cylinder under internal high strain rate loading. *Mechanics of Advanced Materials and Structures*, vol. 24, n. 1, pp. 36–44, 2017.

V. Kats and V. Morozov. High-rated loading, deformation and fracture of thick-walled composite cylinders with an electric explosion of wires. *Procedia Structural Integrity*, vol. 28, pp. 602–607, 2020.

T. dos Santos, P. A. Rosa, S. Maghous, and R. Rossi. A simplified approach to high strain rate effects in cold deformation of polycrystalline FCC metals: Constitutive formulation and model calibration. *International Journal of Plasticity*, vol. 82, pp. 76–96, 2016.

P. Perzyna. Thermodynamic theory of viscoplasticity. volume 11 of *Advances in Applied Mechanics*, pp. 313–354. Elsevier, 1971.

D. Perić. On a class of constitutive equations in viscoplasticity: Formulation and computational issues. *International Journal for Numerical Methods in Engineering*, vol. 36, n. 8, pp. 1365–1393, 1993.

A. Brezolin. Avaliação numérica de um modelo de viscoplasticidade com endurecimento dependente da taxa de deformação. Master's thesis, Universidade Federal do Rio Grande do Sul, Brasil, 2018.

ABAQUS/Standard. *Abaqus Explicit v6.14 User's Manual*. ABAQUS Inc., Richmond, USA, version 6.14 edition, 2020.

T. dos Santos, P. A. Rosa, S. Maghous, and R. Rossi. Numerical modeling of strain rate hardening effects on viscoplastic behavior of metallic materials. In *COMPLAS XIV: proceedings of the XIV International Conference on Computational Plasticity: fundamentals and applications*, pp. 405–435. CIMNE, 2017.

A. Brezolin, T. dos Santos, P. A. Rosa, and R. Rossi. Some numerical verification examples for plane stress elasto-viscoplasticity. In *COMPLAS XV: proceedings of the XV International Conference on Computational Plasticity: fundamentals and applications*, pp. 281–304. CIMNE, 2019.